Alhumairi, M., *et al*.: Active-Grid Turbulence Effect on the Topology and the Flame Location ...
THERMAL SCIENCE: Year 2018, Vol. 22, No. 6A, pp. 2425-2438

2425

ACTIVE-GRID TURBULENCE EFFECT ON THE TOPOLOGY AND THE FLAME LOCATION OF A LEAN PREMIXED COMBUSTION

by

Mohammed ALHUMAIRI[a,b] and Ozgur ERTUNC[a]*

[a] Mechanical Engineering Department, Ozyegin University, Istanbul, Turkey
[b] Engineering College, Diyala University, Diyala, Iraq

Lean premixed combustion under the influence of active-grid turbulence was computationally investigated, and the results were compared with experimental data. The experiments were carried out to generate a premixed flame at a thermal load of 9 kW from a single jet flow combustor. Turbulent combustion models, such as the coherent flame model and turbulent flame speed closure model were implemented for the simulations performed under different turbulent flow conditions, which were specified by the Reynolds number based on Taylor's microscale, the dissipation rate of turbulence, and turbulent kinetic energy. This study shows that the applied turbulent combustion models differently predict the flame topology and location. However, similar to the experiments, simulations with both models revealed that the flame moves toward the inlet when turbulence becomes strong at the inlet, that is, when Re_λ at the inlet increases. The results indicated that the flame topology and location in the coherent flame model were more sensitive to turbulence than those in the turbulent flame speed closure model. The flame location behavior on the jet flow combustor significantly changed with the increase of Re_λ.

Key words: *lean premixed combustion, active-grid turbulence, flame location*

Introduction

Turbulent premixed combustion modeling is essential for various applications, such as gas turbine, spark-ignition engine, and furnace operations, because it helps in improving these technologies to reduce emissions and increase power efficiency. The effects of the turbulent flow field properties of flames are significant because they extremely increase the flame propagation velocity (turbulent flame speed, U_t) [1]. Turbulence can be generated by using an active regular or fractal grid that is placed on the upstream flame region to develop a velocity field [2-4]. The influence of turbulence on combustion is determined by subjecting the flame front to the activity of the eddies to increase the flame surface area, namely, the wrinkling flame [5].

The turbulent combustion models used in this study are coherent flame model (CFM) and turbulent flame speed closure (TFC) model for the reproduction of a turbulent premixed flame under the effect of turbulence generated by an active grid. The turbulence can be modeled by a common k-ε model [6, 7]. The turbulence levels are specified by the turbulent kinetic energy, k, the dissipation rate of turbulence, ε (including turbulent intensity Ti, and turbulent length scale l_t), and the Reynolds number based on the Taylor microscale, Re_λ [8]. Moreover, ε

---

* Corresponding author, e-mail: mohammed.alhumairi@ozu.edu.tr

is the dissipation of k, which is generally defined as the average of the kinetic energy of turbulent velocity fluctuations per unit mass over time. Turbulent intensity generally refers to the turbulence level, which is the ratio between the root mean square of velocity fluctuations u' and mean velocity of the flow. Turbulent intensity has generally critical leverage on the flame surface properties of the diffused flame in the reaction zone below the flame holder surface. Wu *et. al.* [9] reported the effects of varying turbulent intensities on the flame surface position in H_2-air jet flames. They found that the turbulent flame speed and root mean square fluctuation of the flame position increase with distance from the flame holder when the turbulent intensity increases.

Lean premixed combustion in gas turbine burner that use the CFM model was studied by Yilmaz *et. al.* [10]. They used CH_4-air flames with an equivalence ratio, Φ, of 0.6, 0.7, and 0.8, the k-ε turbulence model, and a perforated flame holder to stabilize the flame. They found that the flame brush thickness and the flame length decrease at increasing Φ values. They also found that the modified k-ε turbulence provides better velocity distribution results than the standard k-ε in the region above the burner exit.

Numerical simulations of a laboratory scale rod stabilized V-shaped flame have been implemented by Manickam *et. al.* [11] using TFC model and an algebraic flame surface wrinkling (AFSW) reaction model. They found that the flames angles predicted by the AFSW model are in good agreement with the experiment results, and propane combustion in TFC model shows minimal deviation.

One of combustion products is heat release, which is an essential parameter in the study of turbulent reaction flows. Heat release distribution is useful in understanding flame surface properties and locations in the combustor domain [12, 13]. The heat release from propane and syngas combustion using CFD simulation with STAR-CCM+ software were conducted by Amico [14]. They used the standard k-ε turbulence model and a turbulent intensity 10% for numerical simulation in an adiabatic combustion chamber to generate a 2.3 kW power. They calculated the temperature distribution in the combustor at steady and unsteady conditions and find the propane results were greater than those of the syngas combustion. In addition, the emission measurements from syngas under both steady and unsteady conditions were greater than those of propane. Furthermore, Kanniche and Zurbach [15] used the CFM and the eddy break-up (EBU) models associated to the standard k-ε model to study 2-D turbulent premixed flames. They found that heat release rate is better evaluated by the CFM than by the EBU model.

Understanding the behavior of the flame location and topology in the jet flow combustor with various Re_λ values at a constant thermal load is important in controlling the flame location. Generally, heat release contour visualizes the flame topology. The flame location is assumed to be in the midpoint of the bright region [16]. A few numerical and experimental studies, such as those of Wu *et al.* [9] and Tamadonfar and Gulder [17] examined the turbulence effect on flame location.

The manner in which turbulence behaves upon the influence of the flame location at a constant thermal load and equivalence ratio remains unclear. The flame location is determined by the heat release. A few researchers have investigated the turbulence effect on the flame location [9, 17, 18]. Hartung *et. al.* [18] used an ethylene-air mixture in a circular duct burner. The flame front location was recognized by the maximum concentration of the hydroxyl radical but not by the maximum heat release value. Meanwhile, the flame location changed by altering the equivalence ratio from 0.7 to 1.35 [17]. Moreover, the flame location changed by altering Re_λ, the flame front location was investigated using laser tomography [19]. Although most of these works have been conducted, whether the flame moves downstream or upstream in the combus-

Alhumairi, M., *et al.*: Active-Grid Turbulence Effect on the Topology and the Flame Location ...
THERMAL SCIENCE: Year 2018, Vol. 22, No. 6A, pp. 2425-2438

2427

tor domain by changing the turbulence at a constant thermal load, that is, with a constant velocity mixture in the inlet region. Therefore, a model to predict the behavior of the flame location and topology above the burner exit should be developed by changing Re_λ at a constant thermal load and an equivalence ratio.

Our survey shows that few investigations have been conducted on flame location and topology above the burner exit at various Re_λ values. Therefore, in this work, we calculated the flame location and visualized the flame topology from the heat release of combustion in the jet flow combustor at various Re_λ values without changing the thermal load and geometry. The experimental data were generated with the transverse and longitudinal active regular grids moved by the generated turbulence of 10 motors. A lean premixed flame from propane-air mixture with an equivalence ratio, Φ, of 0.588 was investigated. The CFM and TFC models in STAR CCM+ v10.02 for propane lean premixed combustion were used. A new expression of the turbulent flame speed equation U_t was derived from the Zimont formula in the TFC model. The numerical results were then compared with the experiments parameterized by Re_λ.

Combustion modeling

In the premixed combustion burner, air and fuel were mixed before being sent into the burner. In the CFM and TFC model, the reaction occurs when the combustion region split into unburnt and fully burnt mixtures. The flame front propagation was modeled by solving a transport equation for the reacting progress variable and using the Reynolds-averaged Navier-Stokes (RANS) as in [20]:

$$\frac{\partial \rho Y_f}{\partial t} + \nabla\left(\rho u Y_f\right) = \nabla\left(\Gamma_{Y_f} \nabla Y_f\right) + \omega \tag{1}$$

where Y_f, ρ, and ω are the fuel mass fraction, the density, and source term, respectively. The chemical processes that generated the products and heat in the experiment were described with a single progress variable, which represents a normalized mass fraction of the reactants and products. The chemical source term in propane reaction is the mass of the species, i, produced per unit of time and volume [21, 22]:

$$\omega = \rho_u S_L \Sigma Y_f \quad \text{for CFM model} \tag{2}$$

$$\omega = \rho_u U_t \left|\nabla Y_f\right| \quad \text{for TFC model} \tag{3}$$

where ρ_u is the density of the unburned mixture, S_L – the laminar flame speed, and Σ – the flame surface density, which is written [21]:

$$\Sigma = \left|\nabla c\right| \delta(c - c_f) \tag{4}$$

where $\delta(c - c_f)$ is the site of the instantaneous flame front, and δ is the Kronecker delta. In addition, the combustion occurred inside the flamelet region. Meanwhile, U_t can be computed by using the Zimont formula for the flame front [22]:

$$U_t = AG\left(S_L^{0.5} \alpha_u^{-0.25} u'^{0.75} l_t^{0.25}\right) \tag{5}$$

where A is a TFC model constant, G – the flame stretch factor, and α_u – the unburnt thermal diffusivity of the unburned mixture. The relationship between the root mean square of u' and turbulent kinetic energy k can be written [23]:

$$k = 1.5(u')^2 \tag{6}$$

The turbulent length scale, l_t, can be estimated via the relationship:

$$l_t = \frac{k^{1.5}}{\varepsilon} \frac{C_\mu^{0.75}}{\kappa_v} \tag{7}$$

where ε is the turbulence dissipation rate, κ_v and C_μ are the Von Karman constant and turbulent viscosity coefficient, respectively. The turbulent intensity indicates the turbulence grade in the turbulent combustion and is defined as the ratio between the root mean square values of u' and mean flow velocity $\overline{U}$:

$$Ti = \frac{u'}{\overline{\overline{U}}} \tag{8}$$

Active grids can achieve the high turbulence level, and Reynolds number is used to classify the turbulence strength and it is a Re_λ. In a homogeneous isotropic turbulent flow, it is approximated [6]:

$$\mathrm{Re}_\lambda = k \sqrt{\frac{20}{3v\varepsilon}} \tag{9}$$

By setting the turbulence level through k, ε and Ti at the inlet region for a Re_λ-evaluation, we can determine the flame topology. For comparison, the numerical simulations of CFM and TFC models were conducted at different levels of Re_λ.

The laminar and turbulent flame speeds being important parameters in the CFM and TFC models, we can derive a new expression of the turbulent flame speed U_t depending on the turbulence strength, Re_λ, from eqs. (5)-(9):

$$U_t = 0.4127\, AG\left(v^{0.375} S_L^{0.5} \alpha_u^{-0.25} \mathrm{Re}_\lambda^{0.75}\right) \tag{10}$$

The effect of turbulence on the turbulent flame speed can be represented solely by Re_λ. The constant A in eq. (10) was set at 0.37 in all simulations depending on our prior investigation [24].

Heat release

One way to visualize the flame is to examine the level of heat released, HR, from the combustion. The HR is an essential value for the investigation of turbulent and laminar reacting flows. Practically, the precise distribution of HR inside a combustor is used to observe the flame and determine its location [12]. Many species and radical species are created by burning propane (C_3H_8), beside the heat released. In a completely burned mixture, the entire chemical energy bound in the fuel is transformed into thermal energy. This transformation is called heat release [16], which can be derived from the energy transport equation. When the effect of radiation is disregarded, the energy equation in terms of enthalpy can be written [25]:

$$\frac{\partial \rho h}{\partial t} + \frac{\partial(\rho u_i h)}{\partial x_i} = \frac{DP}{Dt} - \frac{\partial J_i^h}{\partial x_i} + \tau_{ij}\frac{\partial u_i}{\partial x_i} + \omega \tag{11}$$

$$h = \sum_{i=1}^{N}\left\{ Y_i\left[h_i + \int_{T_{ref}}^{T} C_{p,i} T\, dT \right]\right\} \tag{12}$$

Alhumairi, M., *et al.*: Active-Grid Turbulence Effect on the Topology and the Flame Location ...
THERMAL SCIENCE: Year 2018, Vol. 22, No. 6A, pp. 2425-2438

2429

where h is the enthalpy, J_i^h – the enthalpy molecular flux, τ_{ij} – the turbulent stress tensor and $T_{ref} = 298.15$ K is the reference temperature. The temperature is then calculated from ending te state equation.

Every mole of fuel combusted generates an amount of energy from the formation of the species that releases heat. The *HR* produced from the chemical reaction can be written:

$$HR = \sum_{i=1}^{N} h_i \omega \tag{13}$$

where h_i is the low heating value of the fuel and is 46.39 kJ/g for propane. By considering the coupling relation between the species mass fractions and temperature from eqs. (2), (3), and (13), we can write the final expression of *HR* [21]:

$$HR = \int \rho_u S_L \Sigma \Delta H \, dv \quad \text{for CFM model} \tag{14}$$

$$HR = \sum_{i=1}^{n} h_i \, \rho_u U_t \left| \nabla Y_f \right| \quad \text{for TFC model} \tag{15}$$

where ΔH is the enthalpy of the reaction.

Combustion experiments

The combustion experiments were conducted using an active grid, which comprised an array of moving square wings attached to rods and an axisymmetric burner, fig. 1. The active grid generated a high turbulence level with a low flow rate. Ten motors controlled wings' rotation. Experiments were performed to generate a premixed flame at an equivalence ratio, Φ, of 0.588 and approximate Re_λ values of 70, 90, and 110. Table 1 presents the turbulent specifications and inlet flow conditions. The inlet diameter of the burner is 100 mm. The chamber height is 550 mm. The flame holder has a diameter and thickness of 200 mm and 5 mm, respectively, and lies above the burner exit by 100 mm. The mass flow rate of the premixed gas is 5.0868 g/s with an excess air ratio ($\lambda = 1.7$). Air and fuel were mixed before being injected into the chamber, and the mixture included 3.81% C_3H_8, 23.55% O_2, and 72.64% N_2 per mass fraction. The mixture flowed at a constant inlet velocity of 0.484 m/s, that is, constant thermal load of 9 kW. After mixing, the flow was transmitted through a flame barrier and a pipe that encompassed the
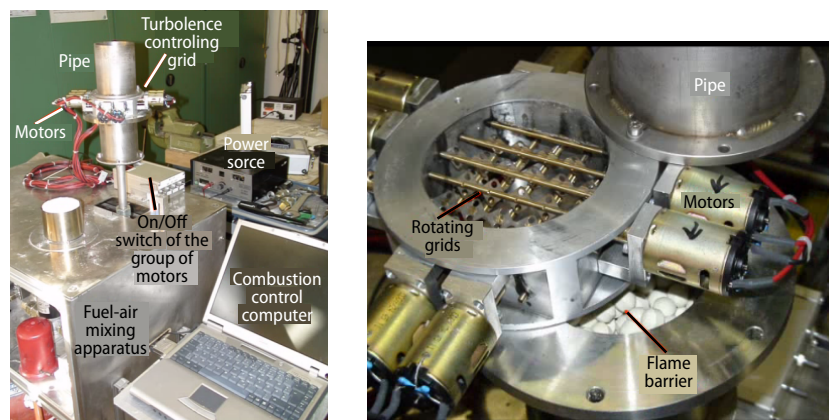

Figure 1. Experimental apparatus (a), an active grids and flame barrier (b)

Table 1. Inlet flow conditions at thermal load of 9 kW

Fuel mass fraction	Oxygen mass fraction	Nitrogen mass fraction	Re_λ	Ti	l_t [m]	k [Jkg^{-1}]	ε [m^{2}s^{-3}]
0.0381	0.2355	0.7264	50	0.5	0.0193	0.0878	1.3475
Equivalence ratio, Φ	TFC constant model, A	Inlet velocity [ms^{-1}]	70	0.5	0.0378	0.0878	0.6882
			90	0.5	0.0625	0.0878	0.4163
				0.5	0.0934	0.0878	0.2787
0.588	0.37	0.484	110	0.608	0.0767	0.13	0.6104
				0.86	0.0542	0.26	2.4416
			130	0.6533	0.0998	0.15	0.58182

transverse and longitudinal active grid to generate turbulent conditions. In the experiment, the flame topology was depicted as low, medium, and highly turbulent depending on the Re_λ. At a low turbulence (*i. e.*, Re_λ = ~70), the flame topology was wrinkled in the domain of the combustor and attached itself to the flame holder surface. However, for a medium turbulence (*i. e.*, Re_λ = ~90), the flame topology remained wrinkled and was located far from the flame holder. At a high turbulence (*i. e.*, Re_λ = ~110), the flame topology was corrugated and moved toward the inlet region. Thus, the increase in turbulent conditions enhanced the heat transfer in the reaction zone for the small eddies of the premixed mixture [26]. The experiments were performed at room temperature and atmospheric pressure. Images extracted from videos were used to capture the flame phenomena. The flame images and their averages can only be used to compare with the numerical simulations due to the limited data of experiments. Turbulence downstream of the active grid was measured with hot-wire anemometer in the absence of combustion. The images were captured using a colored digital camera. Each image is 576 × 720 pixels, representing the flame topology at a specific Re_λ. The images represent an average of 63 instantaneous snapshots of the flame performed by ImageJ techniques with one frame for the first reaction and another frame for the second reaction.

Numerical setup

A 3-D-simulation of the lean premixed combustion was conducted by using the CFM and TFC model are on the basis of finite volume method [22]. All dimensions of the combustion domain were set as the experiment. Along the y-direction, the inlet region is at –0.1 m, the top of the burner exit region is at 0.0 m, and the bottom surface of the flame holder is at 0.1 m. In the CFM, the determination of the reaction rate, see eq. (2), depends on the consumption rate of the fuel per unit area of the flame and flame surface density [23]. For another promising and interesting model, namely, the TFC model, we modified the Zimont correlation [27] for U_t, eq. (5), and derived a new expression for U_t, eq. (10). This equation was used to determine *HR* in the same manner as for eq. (15), which represents the flame topology and reflects the design, performance, and accuracy of the model. The propane-air reaction with steady-state solution was used in both models. The Gulder correlation for propane was used for S_L-correlation in both models. For the turbulence characteristics, the second-order upwind convection scheme and the segregated flow for viscous regime for both models were used [22]. The grid is an unstructured polyhedral mesh, and the smallest cell diameter is 0.88 mm for M4. Figure 2 shows the cross-section of the axisymmetric combustor dimensions.

Figures 3 and 4 show the results of the grid dependency study based on the flame location. Flame locations are calculated by CFM and TFC models from the maximum heat release

value on the centerline of the combustor at $Re_\lambda = 70$ with different mesh numbers. Therefore, various grid numbers, from M1 (*i. e.*, coarse mesh) to M9 (*i. e.*, fine mesh), were tested in the jet flow combustor domain to check the optimal mesh density. Table 2 presents the mesh numbers and flame locations of grid independency analyses. In the CFM, the flame location decreased gradually with the increase in mesh number from M1 to M3 and did not vary with the decrease in mesh size after M4. Therefore, the flame location converged to a solution and became independent of the mesh size. The same process occurred with the TFC model. From about 300000 grid cells, for mesh number M4 and beyond, the flame location did not vary for both models to an extent that would have influenced the derived conclusions. Therefore, the following simulations were performed by using M4 for 301594 grid cells. In addition, the deviations in the flame locations are 2 mm and 3 mm between coarse and fine meshes of the CFM and TFC models, respectively.

Figure 2. Combustion chamber section and the mesh

We investigated the flame topology at $Ti = 50\%$, $k = 0.0878$ J/kg, and $Re_\lambda = 50, 70, 90, 110,$ and 130. We then tested the flame topology at $Re_\lambda = 110$ and turbulent intensities of 60% and 86% for $k = 0.13$ and 0.26 J/kg, respectively. The flame topologies and locations were visualized using the calculated amount of heat released from propane burning inside the combustor domain.

Table 2. Grid independency analysis results

Mesh number	Cells number	Flame location CFM model [m]	Flame location TFC model [m]
M1	174592	0.09600	0.05600
M2	235976	0.09550	0.05700
M3	268836	0.09480	0.05880
M4	301594	0.09431	0.05901
M5	340595	0.09422	0.05905
M6	437730	0.09418	0.05921
M7	568607	0.09413	0.05928
M8	774058	0.09409	0.05935
M9	981745	0.09405	0.05940

All numerical simulations were performed with the STAR CCM+.02 software [22]. The boundary conditions of all the combustor parts, such as the velocity inlet condition in the
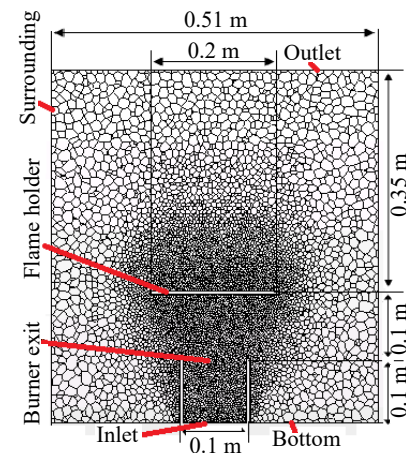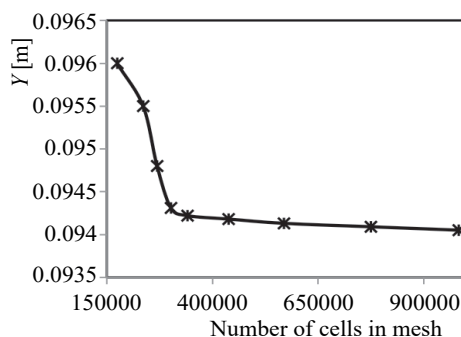

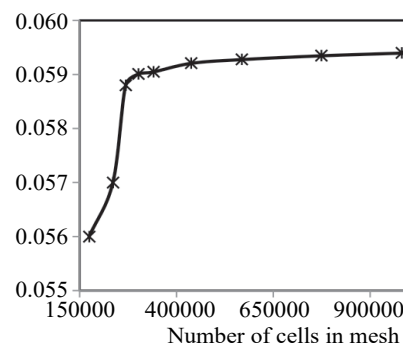**Figure 3. Flame location at $Re_\lambda = 70$ with different number of the mesh in CFM**

Figure 4. Flame location at $Re_\lambda = 70$ with different number of the mesh in TFC model

inlet region and the pressure outlet in the outlet regions were used. The realizable k-ε two-layer model was used for turbulence modeling [28].

Results and discussion

The CFM and TFC models are used to simulate the premixed combustion of the propane-air reaction. The turbulent combustion regimes can be characterized by consid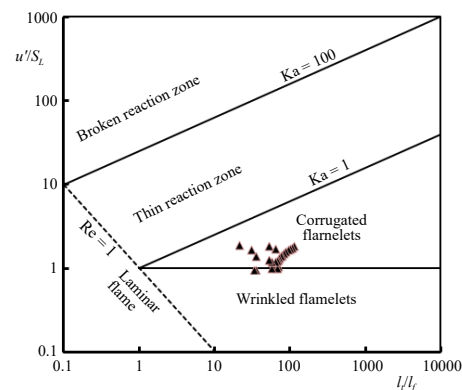ering the relationship between the turbulent and chemical reaction scales. This relationship involves several dimensionless numbers in the analysis. One of such numbers is the Karlovitz number, Ka, which is an key parameter in the Borghi diagram [29]. The Ka is the ratio of chemical time scale and smallest turbulent time scale [30]. In this study, the combustion occurs in the wrinkled and corrugated flamelet regions. Figure 5 presents the flame locations on the Borghi diagram in the flamelet regions.

Figure 6 shows the experimental averaged flame images of a premixed gas mass flow rate at 5.0868 g/s and an excess air ratio ($\lambda = 1.7$) at a different Re_λ and 300 K. The images represent the flame topologies and locations at different Re_λ values (*i. e.*, $Re_\lambda = 70$, 90, and 110). The images represent an average of 63 instantaneous snapshots of the flame performed by ImageJ techniques. Generally, the flames are blue and corrugated, and move upstream toward the burner exit by increasing Re_λ due to complete fuel burning. The flame may flash back with a further turbulence increase. The flame barrier prevents this incident. However, the gas is stopped to prevent the active grid, located above the flame barrier, from being damaged. In addition, sufficient amount of oxygen in the fuel molecule of premixed gas facilitates the oxidation of the fuel, thereby increasing the homogeneous combustion area below the flame holder and preventing soot formation.

Figure 5. Flame locations on the premixed turbulent combustion regime (Borghi diagram [29]

Re$_\lambda$ ~ 70   Re$_\lambda$ ~ 90   Re$_\lambda$ ~ 110
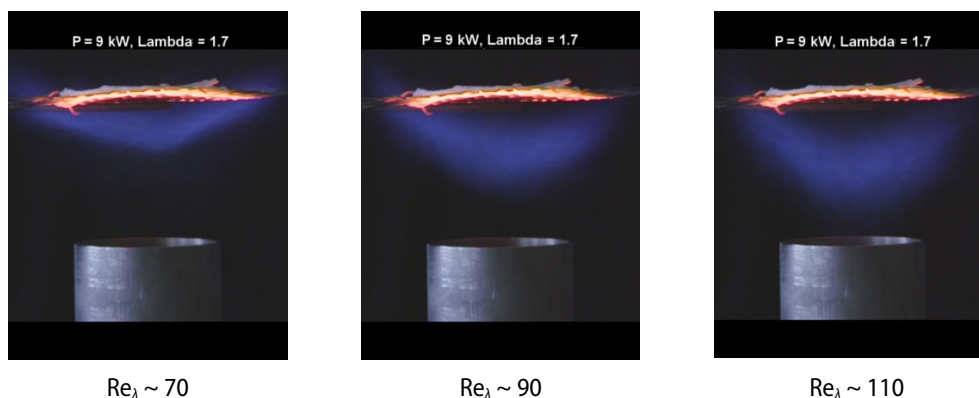
Figure 6. Average of 63 instantaneous snapshots of experimental flame images at excess air ratio ($\lambda = 1.7$), and shows the stages of increasing Re$_\lambda$ (*for color image see journal web site*)

Alhumairi, M., *et al.*: Active-Grid Turbulence Effect on the Topology and the Flame Location ...
THERMAL SCIENCE: Year 2018, Vol. 22, No. 6A, pp. 2425-2438

2433

Figure 7 shows the comparisons between the CFM and TFC models for simulated average heat releases from eqs. (14) and (15) and velocity streamlines at different Re_λ values. Generally, the flame location moves to the inlet region and far from the flame holder (as can be seen also from the *HR* taken from the centerline of the combustor figs. 8 and 9). When $Re_\lambda = 70$, the CFM flame topology appears as a mushroom and has less diffusion toward the inlet region. However, the flame topology of the TFC model is symmetric and remains in contact with the burner exit. Moreover, at $Re_\lambda = 90$ and 110, the flame topology predicted by the CFM appears to be more diffusive than that predicted by the TFC model. The flame locaon moves from the flame holder toward the inlet region. In addition, although *Ti* remains constant at 50% three different Re_λ values, the turbulent length scale l_t is large at $Re_\lambda = 110$. The influence of the
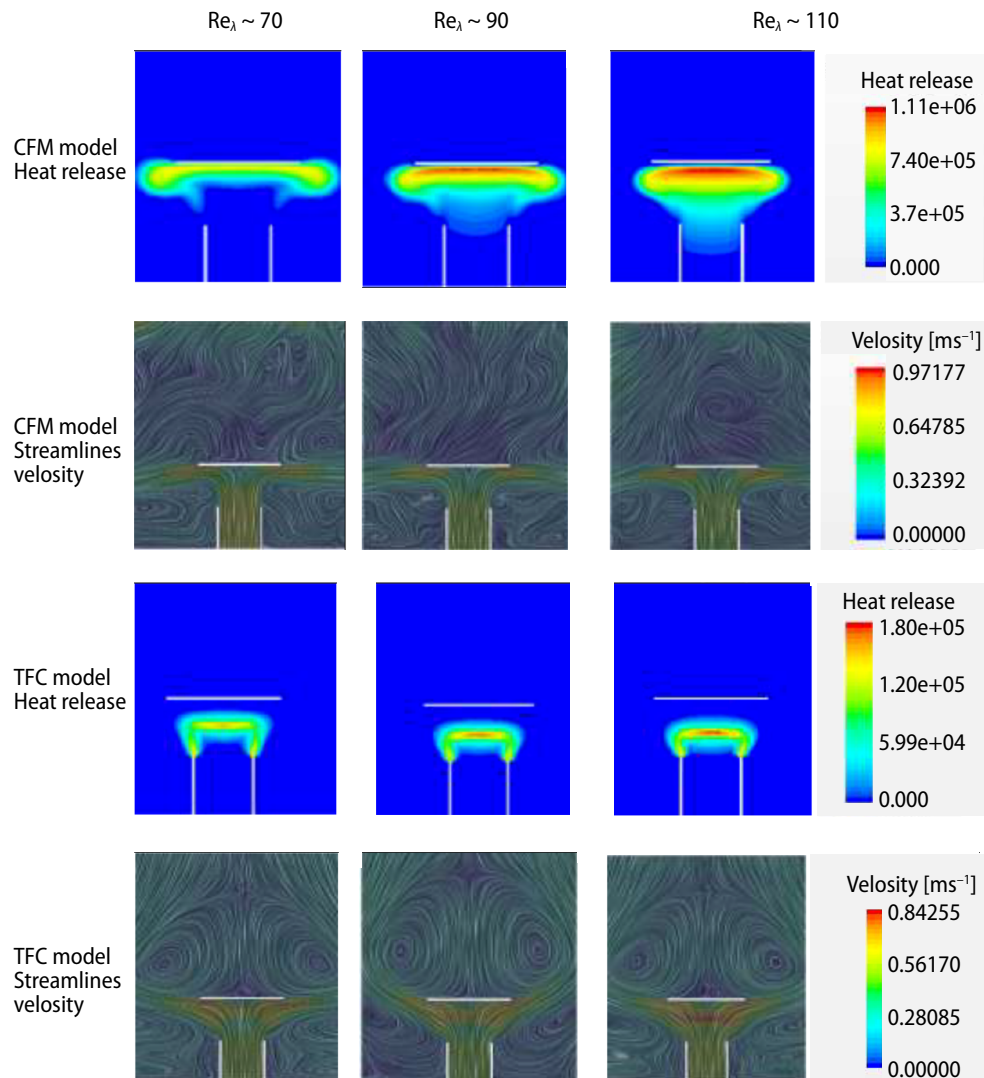

Figure 7. The average heat release and velocity streamline contours of CFM and TFC models at different Re_λ (*for color image see journal web site*)

length scale depicts itself as a thickened combustion region for the CFM model, whereas the TFC model shows less sensitivity to the changes in l_t. Furthermore, the distribution of velocity streamlines of the CFM and TFC models is presented in all combustor domains and significantly show that the flame location affects the re-circulation zone behind the flame holder. The reverse flow is more affected in the CFM model than in the TFC one, which causes the spread of the flame toward the inlet region.

Figures 8 and 9 presents the average HR distribution in the axial direction of the combustor at Re_λ of 70, 90, 110, and 130, coming from CFM and TFC models, respectively. The profile curves show significantly that the flame moves upstream of the flame front with the increase of Re_λ. However, at all values of Re_λ, the maximum HR calculated by the CFM model is higher than that of the TFC model. At high Re_λ, the CFM model simulations show more flame spread toward the inlet region than those using the TFC model. In accordance with the equations of the heat release, eqs. (14)-(15), the TFC model depends on the turbulent flame speed, whereas the CFM depends on the laminar flame speed. Therefore, large differences can be observed in flame thickness and location calculations using these two models.
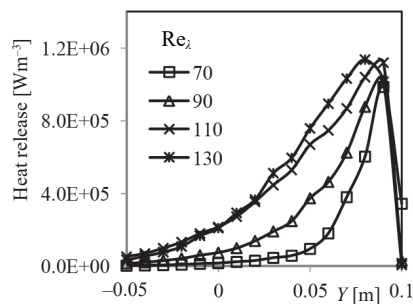

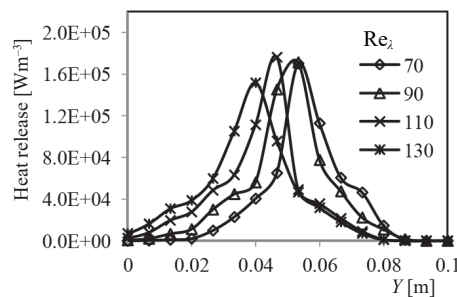**Figure 8. The *HR* calculated by the CFM at different Re$_\lambda$**

Figure 9. The *HR* calculated by the TFC model at different Re$_\lambda$

Figure 10 shows the flame location along the centerline of the combustor above the burner exit calculated at the maximum heat release value in the reaction region. The flame location decreases gradually with the increase in Re_λ. The flame gradually moves upstream of the flame front toward the burner exit with the increase in Re_λ. The flame in the TFC model moves downward more than that in the CFM model toward the inlet region. This tendency indicates the increase of the reaction rate due to an increase in the flame temperature. This observation on the flame location is consistent with the experimental results.

Figure 11 shows the temperature distributions of the TFC model in the centerline of the combustor. In all simulations, the peak temperature reaches 1740 K. Interestingly, a growing trend is observed in the average temperatures obtained in the zone below the flame holder. No significant difference is observed among the average temperature profiles of propane-air flames at Re_λ = 70, 90, 110, and 130 at y = 0.0 m, that is, at the burner exit. However, differences at y = 0.05 m are observed in the TFC mod. Therefore, an increase of Re_λ changes the turbulent conditions from weak to strong cases, thereby pulling combustion toward the inlet. The improved mixing between the premixed propane-air mixtures causes this result.

To distinguish the influence of turbulent kinetic energy on the flame topology and location, simulations with k = 0.0878, 0.13, and 0.26 J/kg at the inlet but at Re_λ. =110 are conducted only with the TFC model. Figures 12 and 13 show the developments of k and HR, respectively. In fig. 12, despite the variations of k values in the inlet region (*i. e.*, y = –0.1 m) and
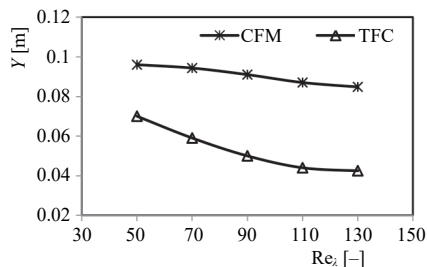
Alhumairi, M., *et al.*: Active-Grid Turbulence Effect on the Topology and the Flame Location ...
THERMAL SCIENCE: Year 2018, Vol. 22, No. 6A, pp. 2425-2438

2435

Figure 10. Flame location of the CFM and TFC models at different Re_λ
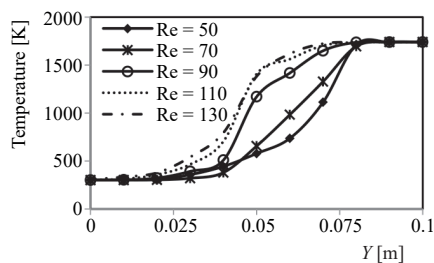

Figure 11. Temperature distribution extracted from the simulations conducted by TFC model at different Re_λ

$Re_\lambda = 110$ (high turbulence), the high k value (0.26 J/kg) decreases more rapidly in the cold flow region than 0.0878 J/kg and 0.13 J/kg values. However, they have the same trend in the hot flow region, particularly in the region below the flame holder at $y = 0$-0.1 m, after combustion occurs. Thus, the flame topology and location are not affected by the change of k values or turbulence dissipation rate when Re_λ is constant. Only the maximum value of *HR* decreases with the increase of k as shown in fig. 13. These results confirm eq. (10), which indicates that the turbulent flame speed can vary depending on the Re_λ. Only this variation can determine the flame locaon.
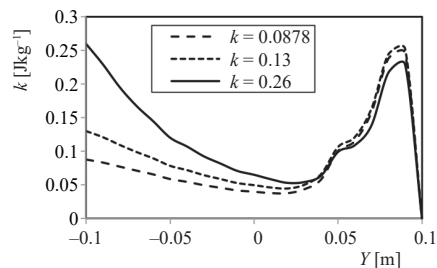

Figure 12. The distribution in the axial direction of the combustor by the TFC model at $Re_\lambda = 110$
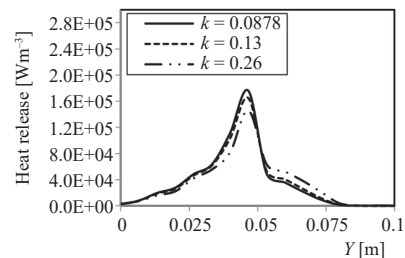

Figure 13. The *HR* calculated by the TFC model at $Re_\lambda = 110$ and different k

Figure 14 shows the distribution of the mean flow velocity in the axial direction of the combustor at different Re_λ values. In general, in the inlet region (*i. e.*, $y = -0.1$ m), the mean velocity of 0.484 m/s gradually increases to approximately 0.5 m/s at the burner exit and then decreases due to an expansion area. After combustion, the average velocity increases rapidly to a maximum value, then decreases to a minimum value at the stagnation point at the flame holding zone (*i. e.*, $y = 0.1$ m).

Figure 15 shows the distribution of the turbulent flame speed, U_t along the centerline of the combustor of the TFC model at different Re_λ values and at $k = 0.0878$. The turbulent flame speed increases with the Re_λ and at a constant k in the inlet region, in accordance with eq. (10). In all cases tested, U_t initially decreases from the turbulence dynamics, as expected, and then suddenly increases within the flame zone. The increase of U_t that occurs within the zone of the combustion starts at $y = 0.02$ m above the burner exit. The maximum heat release value can be determined by changing U_t and subsequently the flame location.
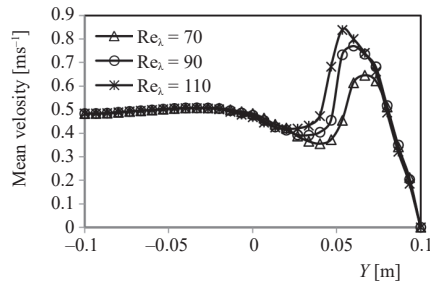
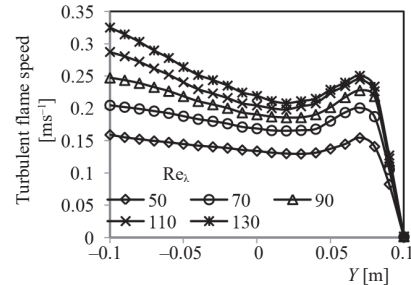**Figure 14. Mean velocity distribution along centerline of the combustor of TFC at different Re_λ**

Figure 15. The U_t distribution along centerline of the combustor of TFC at different Re_λ

Conclusions

The characteristics of the turbulent premixed flame and flame location were examined through the CFM and TFC model with $Re_\lambda = 50, 70, 90, 110$, and 130. The average heat release, velocity streamline of the flow, temperature, turbulent kinetic energy, turbulent flame speed, and flame location were measured. At a low Re_λ value, the flame topology was wrinkled and symmetric with respect to the vertical axis of the combustor, whereas at medium and large Re_λ values, the flame topology exhibited cusps. Generally, the flame was not confined between the burner exit and flame holder in the same manner as that observed in the experiment; however, it attempted to diffuse toward the inlet region. Any increase in Re_λ allowed the flame to move upstream toward the burner exit. However, the CFM and TFC model produced a different flame topology. The results showed that the flame in the CFM diffused more into the inlet region than that in the TFC model by increasing Re_λ. This observation enhanced the experimental results of transport small turbulent eddies, thereby enhancing combustion by increasing the flame area.

Flame location and topology did not show any dependence on turbulent kinetic energy at a constant Re_λ. The results showed that the flame location and topology were influenced solely by Re_λ, as suggested by the derived equation for U_t.

Acknowledgments

Nomenclatures

A	– TFC model constant, [–]	k	– turbulent kinetic energy, [Jkg^{-1}]
C_μ	– turbulent viscosity coefficient, [–]	l_f	– laminar flame length scale, [m]
c	– progress variable, [–]	l_t	– turbulent length scale, [m]
c_p	– specific heat at constant pressure, [Jkg^{-1}K^{-1}]	p	– pressure, [Pa]
G	– flame stretch factor	Re_λ	– Reynolds number based on
HR	– heat release, [Wm^{-3}]		Taylor microscale, [–]
ΔH	– enthalpy of the reaction, [Jmol^{-1}]	S_L	– laminar flame speed, [ms^{-1}]
h	– enthalpy	T	– temperature, [K]
h_i	– lower heating value of propane, [kJg^{-1}]	T_{ref}	– reference temperature, [K]
J_i^h	– molecular flux of enthalpy	Ti	– turbulent intensity, [%]
Ka	– Karlovitz number, [–]	U_t	– turbulent flame speed, [ms^{-1}]

Alhumairi, M., *et al.*: Active-Grid Turbulence Effect on the Topology and the Flame Location ...
THERMAL SCIENCE: Year 2018, Vol. 22, No. 6A, pp. 2425-2438

2437

$\overline{U}$ – the local mean velocity of the flow, [ms^{-1}]
u – axial velocity, [ms^{-1}]
u' – rms of turbulent fluctuation velocity, [ms^{-1}]
Y_f – fuel mass fraction

Greek symbols

δ – Kronecker delta
ε – dissipation rate of turbulence, [m^2s^{-3}]

λ – thermal conductivity, $Wm^{-1}K^{-1}$]
ν – turbulent viscosity, [m^2s^{-1}]
ρ – density, [kgm^{-3}]
ρ_u – unburned density of the mixture, [kgm^{-3}]
Σ – flame surface density, [m^{-1}]
τ_{ij} – turbulent stress tensor
Φ – equivalence ratio, [–]
ω – source term

References

[1] Sponfeldner, T., *et al.*, The Structure of Turbulent Flames in Fractal- and Regular-Grid-Generated Turbulence, *Combust. Flame*, *162* (2015), 9, pp. 3379-3393
[2] Mydlarski, L.,Warhaft, Z., On the Onset of High-Reynolds-Number Grid-Generated Wind Tunnel Turbulence, *J. Fluid Mech.*,*320* (1996), 1, pp. 331-368
[3] Soulopoulos, N., *et al.*, Turbulent Premixed Flames on Fractal-Grid-Generated Turbulence, *Fluid Dyn. Res., 45* (2013), 6, pp. 1-18
[4] Goh, K., *et al.*, Lean Premixed Opposed Jet Flames in Fractal Grid Generated Multiscale Turbulence, *Combust. Flame*, *161* (2014), 9, pp. 2419-2434
[5] Gulder, O. L. ,Yuen, F. T. C., Turbulent Premixed Flame Front Dynamics and Implications for Limits of Flamelet Hypothesis, *Proc. Combust. Inst.*, *34* (2013), 1, pp. 1393-1400
[6] Ozdemir, I. B, Use of Computational Combustion in the Development and Design of Energy-Efficient Household Cooker-Top Burners, *J. Energy Resour. Technol. ASME*, *139* (2016), 2, pp. 22206-22208
[7] Muppala, F. D. S., Manickam, B., A Comparative Study of the Different Reaction Models for Turbulent Methane-Hydrogen-Air, *J. Therm. Eng.*,*1* (2015), 1, pp. 367-380
[8] Pope, S. B. , *Turbulent Flows*, Cambridge Univ. Press, Cambridge, UK, 2000
[9] Wu, M. S. , *et al.*, Preferential Diffusion Effects on the Surface Structure of Turbulent Premixed Hydrogen/Air Flames, *Combust. Sci. Technol.*, *78* (1991), Feb., pp. 69-96
[10] Yilmaz, B., *et al.*, Numerical Study of Turbulent Lean Premixed Methane-Air Flames, *Fuels Combust. Eng. J.*, *1* (2015), pp. 26-33
[11] Manickam, B., *et al.*, Numerical Simulation of Rod Stabilized Flames, *V. Eur. Conf. Comput. Fluid Dyn. Eccomas CFD*, (2010), June, pp. 14-17
[12] Nikolaou, Z. M. , Swaminathan, N. , Heat Release Rate Markers for Premixed Combustion, *Combust. Flame*, *161* (2014), 12, pp. 3073-3084
[13] Schmid, H., *et al.*, A Model for Calculating Heat Release in Premixed Turbulent Flames, *Combust. and Flame*, *113* (1998), 97, pp. 79-91
[14] Amico, M. E., CFD Simulation of a Burner for Syngas Characterization: Preliminary Results and Experimental Validation, *Proceedings*, 18th Eur. Biomass Conf. Exhib., Lion, France, 2010, pp. 3-7
[15] Kanniche, M., Zurbach, S., Coherent Flame Model for Turbulent Combustion Operatıng with Both Premixed and Non-Premixed Flames, *ASME Journal, Present. Int. Gas Turbine Aeroengine Congr. Expo.*, *95* (1995), 95-GT-168
[16] Law, C. K., *Combustion Physics,* Cambridge Univ. Press, Cambridge, UK, 2006
[17] Tamadonfar, P. , Gulder, O. L., Effects of Mixture Composition and Turbulence Intensity on Flame Front Structure and Burning Velocities of Premixed Turbulent Hydrocarbon/Air Bunsen Flames, *Combust. Flame*, *162* (2015), 12, pp. 4417-4441
[18] Hartung, G., *et al.*, Effect of Heat Release on Turbulence and Scalar-Turbulence Interaction in Premixed Combustion, *Phys. Fluids*, *20* (2008), 3, pp. 1-17
[19] Mazellier, N., *et al.*, Multi-Scale Turbulence Injector: A New Tool to Generate Intense Homogeneous and Isotropic Turbulence for Premixed Combustion, *J. Turbul.*, *11* (2010), 2, pp. 1-30
[20] Swaminathan, N., Bray, K. N. C., *Turbulent Premixed Flames*, Cambridge Univ. Press, Cambridge , UK, 2011
[21] Gulder, O. L., Smallwood, G. J., Flame Surface Densities in Premixed Combustion at Medium to High Turbulence Intensities, *Combust. Sci. Technol.*, *179* (2007), 1, pp. 191-206
[22] ***, CD-adapcoTM, CD-adapco, STAR CCM+ Documentation and User Guide, Version 11.02.009-R8., Melville, USA, 2016
[23] Meneveau, C., Poinsot, T., Stretching and Quenching of Flamelets in Turbulent Premixed Combustion, *Combust. Flame*, *86* (1991), pp. 311-332

[24] Alhumairi, M., Ertunc, O., The Calibration of Turbulent Flame Speed Closure Model to Predict the Premixed Combustion Flame under the Influence of Weak to Strong Turbulence, *Proceedings*, Int. Conf. Energy Therm. Eng. Istanbul 2017, pp. 1-7

[25] Kuo, K. K., Acharya, R., *Fundamentals of Turbulent and Multi-Phase Combustion,* John Wiley and Sons, Inc., Hoboken, N. J., USA, 2012

[26] Yuen, F. T., Gulder, O. L., Investigation of Dynamics of Lean Turbulent Premixed Flames by Rayleigh Scattering, *AIAA J.*, *47* (2009), 12, pp. 2964-2973

[27] Zimont, V., An Efficient Computational Model for Premixed Turbulent Combustion at High Reynolds Numbers Based on a Turbulent Flame Speed Closure, *J. Eng. Gas Turbines Power*, *120* (1998), 3, 97-GT-S95

[28] Shih, T. H., *et al*., A New k-ε Eddy Viscosity Model for High Reynolds Number Turbulent Flows: Model Development And Validation, *Comput. Fluids*, *24 (1995)*, Aug., pp. 227-238

[29] Kheirkhah , S. ,Gulder, L., Topology and Brush Thickness of Turbulent Premixed V-shaped Flames, *Flow, Turbul. Combust.*, *93* (2014), 3, pp. 439-459

[30] Salusbury, S. D., Experiments in Laminar and Turbulent Premixed Counter-Flow Flames at Variable Lewis Number, Ph. D. thesis, McGill University, Montreal, Canada, 2014